1 of 1

Conf-931168--61

PNL-SA-22766

DEFECT-SOLUTE INTERACTIONS NEAR IRRADIATION GRAIN BOUNDARIES

E. P. Simonen
J. S. Vetrano
H. L. Heinisch
S. M. Bruemmer

November - December 1993

Presented at the
MRS Fall 1993 Meeting
November 29 - December 3, 1993
Boston, Massachusetts

Work supported by
the U.S. Department of Energy
under Contract DE-AC06-76RLO 1830

Pacific Northwest Laboratory
Richland, Washington 99352

DEFECT-SOLUTE INTERACTIONS NEAR IRRADIATED GRAIN BOUNDARIES

E. P. SIMONEN*, J. S. VETRANO*, H. L. HEINISCH* AND S. M. BRUEMMER*
*Pacific Northwest Laboratory, P. O. BOX 999/ F8-15, Richland, WA 99352

ABSTRACT

Defect-solute interactions control radiation-induced segregation (RIS) to interfacial sinks, such as grain boundaries, in metallic materials. The best studied system in this regard has been austenitic stainless steels. Measurements of grain boundary composition indicate that RIS of major alloying elements are in reasonable agreement with inverse-Kirkendall predictions. The steep and narrow composition profiles are shown to result from limited back diffusion near the boundary. Subsequently, defect-solute interactions that affect the near boundary defect concentrations strongly affect RIS. The variability in measured RIS may in part be caused by grain boundary characteristics.

INTRODUCTION

Point-defect (vacancy and interstitial) flow and defect-solute interactions cause change in solute concentration near grain boundaries during irradiation [1]. This effect is known as radiation-induced segregation (RIS). The magnitude of RIS depends on both the intensity of the defect flux to a grain boundary and the strength of coupling between defect flux and solute [2,3]. For austenitic stainless steels, both irradiation and thermal annealing responses are consistent with assumptions of slow Ni diffusion and fast Fe and Cr diffusion rates [4]. Grain boundary enrichment of slow diffusing Ni and depletion of fast diffusing Cr and Fe are observed and are consistent with inverse-Kirkendall diffusion and a vacancy mechanism for RIS.

Material characteristics as well as irradiation parameters affect the magnitude of vacancy flux to grain boundaries [5]. Matrix characteristics include defect sink density, kinetics of vacancy migration and strength of interaction between defects and solutes. Irradiation characteristics include the irradiation temperature and the irradiation particle flux, dose, and damage efficiency.

In this paper, the effects of neutron and charged-particle irradiation on RIS in Fe-Cr-Ni stainless steels are examined. The defect-solute coupling is assumed to be associated with vacancy flow to grain boundaries. Model predictions are used to demonstrate expected conditions for influence of grain boundary sink efficiency , near-grain-boundary influence and matrix influence on segregation responses. Predicted RIS is compared to measured grain boundary compositions to interpret damage efficiencies and possible influences of defect-solute interactions near irradiated grain boundaries.

THEORETICAL APPROACH

Point-defect rate theory has been used to predict defect flow to irradiated grain boundaries and has included coupling of the defect flow with solute to induce RIS [6]. Rate equations describe the production, annihilation and migration of vacancies and interstitials, and the subsequent migration of solute coupled to defect flow. Vacancy, v, and interstitial, i, reactions are described by the following diffusion equations accounting for the defect production rate, K, and the defect loss rates caused by mutual recombination, R_r, and annihilation at sinks, $R_{(v,i)}$.

$$\frac{dC_v}{dt} = -\frac{d}{dx}\left[C_v \sum_k \left(d_{kv}\alpha\frac{dC_k}{dx}\right) - D_v\frac{dC_v}{dx}\right] + K + K' - R_r - R_v \qquad (1)$$

and

$$\frac{dC_i}{dt} = -\frac{d}{dx}\left[C_i \sum_k \left(d_{ki}\alpha\frac{dC_k}{dx}\right) - D_i\frac{dC_i}{dx}\right] + K - R_r - R_i \qquad (2)$$

The thermodynamic parameter, α, is unity; K is the product of the atomic displacement rate and the damage efficiency; and K' is the thermal emission rate of vacancies from sinks.

For a model ternary alloy similar to austenitic stainless steel, diffusion of solute k (Fe, Cr, and Ni) is described by

$$\frac{dC_k}{dt} = -\frac{d}{dx}\left[D_k\alpha\frac{dC_k}{dx} + C_k\left(d_{kv}\frac{dC_v}{dx} - d_{ki}\frac{dC_i}{dx}\right)\right]. \qquad (3)$$

Total diffusivities, D_k, and partial diffusivities, $d_{k(v,i)}$ are defined by Perks et al [6].

Simultaneous solutions to Equations 1-3 provide predictions of solute redistribution induced by radiation-induced defect fluxes to grain boundaries and solute interactions with those defect fluxes. Finite difference numerical methods have been used to solve the above equations. In the present calculations, the GEAR numerical subroutines [7] were used. Material constants were selected to be consistent with those assumed by Perk's et al. except when noted. A dislocation density of 10^{14} m^{-2} was assumed. Alloy compositions and irradiation conditions were selected to represent conditions for experimentally measured segregation responses.

CALCULATED RIS CONCENTRATION PROFILES

RIS can be characterized by measuring the concentration profiles of solute near grain boundaries for selected irradiations of specific alloys. The observed radiation-induced enrichment of Ni, and depletion of Cr and Fe, in austenitic stainless steels have been attributed to the slow diffusion of Ni compared to fast diffusion of Cr and Fe. Perks et al. [6] have based the differential solute diffusion rates on measured changes in concentration profiles during annealing. In the present analysis of several examples of RIS in austenitic steels, it was found that an adjusted 20% increase in the assumed Fe diffusivity compared to Perks et al. resulted in better agreement between model predictions and measured RIS behavior compared to the predictions of Perks et al. The assumed Fe diffusivity was 2.01 times faster than Ni and the assumed Cr diffusivity was 2.55 times faster than Ni.

Causes for Nanoscale Profiles

Calculated solute concentration profiles are narrower and steeper than are the vacancy profiles that induce RIS. Predicted and measured solute concentration profiles are only a few nms in size, whereas predicted vacancy concentration profiles are tens to hundreds of nms in size. A comparison of calculated solute concentration and vacancy concentration (normalized to unity at 20 nm) is shown in Figure 1a for the case of neutron irradiation of a 304SS to 2 dpa at 288°C. The Cr concentration increases rapidly with distance from the grain boundary, while the vacancy concentration shows a comparatively gradual increase on this normalized scale. However, a much clearer comparison is identified by comparing the Cr concentration gradient to the inverse vacancy concentration in Figure 1b. The Cr concentration gradient,which controls the thermodynamic driving force for Cr back diffusion, changes over the same dimensional scale as the inverse vacancy concentration that controls the kinetics of back diffusion.

The steep and narrow Cr concentration gradient shown in Figure 1 indicates the challenge for measuring profiles that change rapidly over a few nms. Field-emission-gun, scanning-transmission-electron-microscopy (FEG-STEM) has been used to measure chromium concentration profiles near grain boundaries. Because the probe resolution is comparable to widths of the RIS zone, predictions must account for the dimensional limits of the analysis probe. The predicted grain boundary concentrations reported in this paper are those for an expected FEG-STEM measurement using a 2 nm incident beam that has a 3 nm through-thickness size. The beam profile was assumed to be Gaussian with 85% of the beam inside the probe size (3 nm).

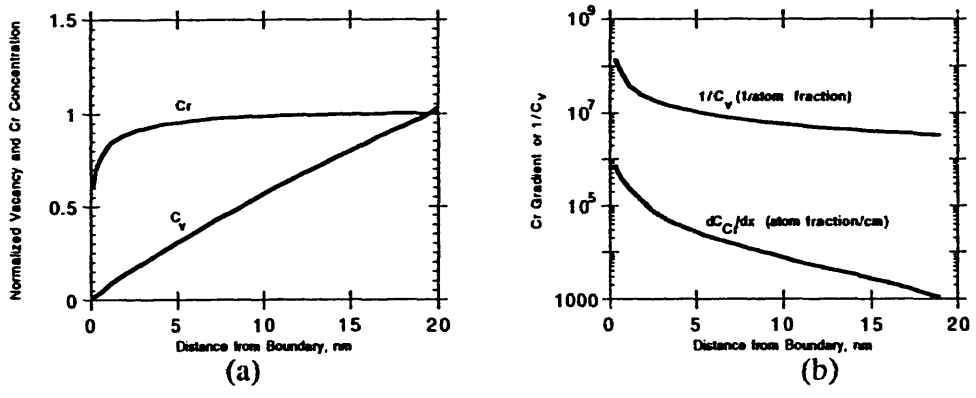

Figure 1. The calculated Cr depletion profile does not correlate with the vacancy profile (a) but the Cr concentration gradient does correlate with the inverse vacancy concentration(b). The lack of back diffusion at the boundary causes steep Cr concentration gradients near the boundary.

Parameter Sensitivities

The matrix irradiation and material characteristics, namely, the production and survival of freely migrating defects, control the potential for RIS. The atomic displacement rate and the damage efficiency for survival of freely migrating defects establishes the initial number of defects that can contribute to RIS. The two primary vacancy and interstitial loss mechanisms include mutual recombination and annihilation at matrix sinks. These irradiation and material characteristics establish the potential for vacancy flux to grain boundaries. For a given coupling of defects to solutes, changes in the vacancy flux cause similar changes in the RIS profiles independent of the cause for change in the vacancy flux. Changes in the model assumption for damage efficiency, dislocation density and vacancy mobility have equivalent effects on the RIS profiles as shown in Figure 2. Higher damage efficiencies, lower dislocation densities and faster vacancy mobilities promote higher defect fluxes to grain boundaries. The profiles progress to greater depletion minimums and greater depletion widths as assumptions are changed to promote greater vacancy flux to the grain boundary.

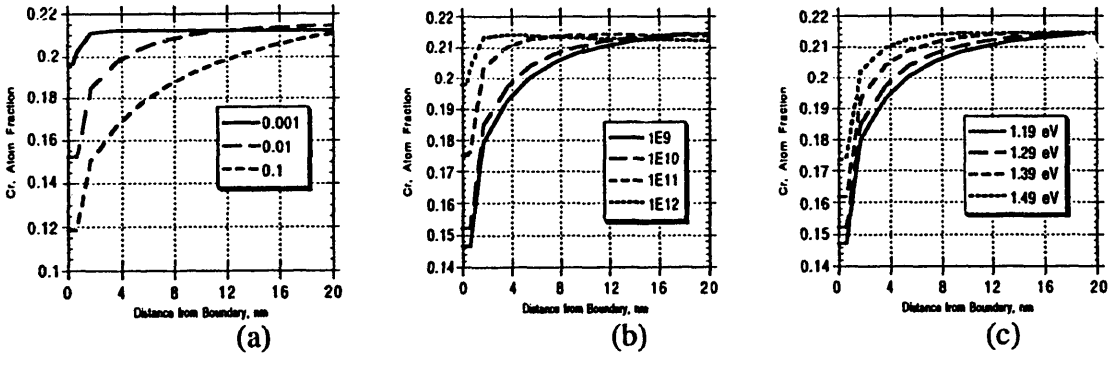

Figure 2. The effects of changing the assumed damage efficiency (a), matrix dislocation density (b) and vacancy migration energy (c) on calculated chromium depletion profiles. The reference values in this paper are a damage efficiency of 0.03, 10^{10} dislocations/cm^2 and 1.29 eV.

The above sensitivity calculations assume that the matrix characteristics are uniform near and far from the boundary and that the grain boundaries act as perfect sinks, i.e., are independent of rate processes at the grain boundary. Two thermally activated processes that occur at grain boundaries include thermal emission of vacancies in excess of that assumed by equilibrium thermodynamics

and an activation barrier for defect accommodation in the boundary that is different from the matrix jump activation barrier for vacancies. As illustrated in Figure 1b, the local vacancy concentration at grain boundaries has a strong influence on the local Cr concentration gradient.

The effect of assumed activation energy for formation of vacancies and the effect of an additional activation barrier for vacancy jumps into the boundary are shown in Figure 3a. Effects of neutron irradiation at low temperature, 300°C, and at high temperature, 500°C, are shown. The calculations indicate that significant changes in vacancy formation energy are necessary to cause significant influence on RIS, whereas lesser changes in kinetic activation barriers cause significant influence on RIS. This behavior depends on temperature and damage rate. Vacancy formation energy is more significant at high temperature and low damage rate. Kinetic barriers are more significant at low temperature and high damage rate.

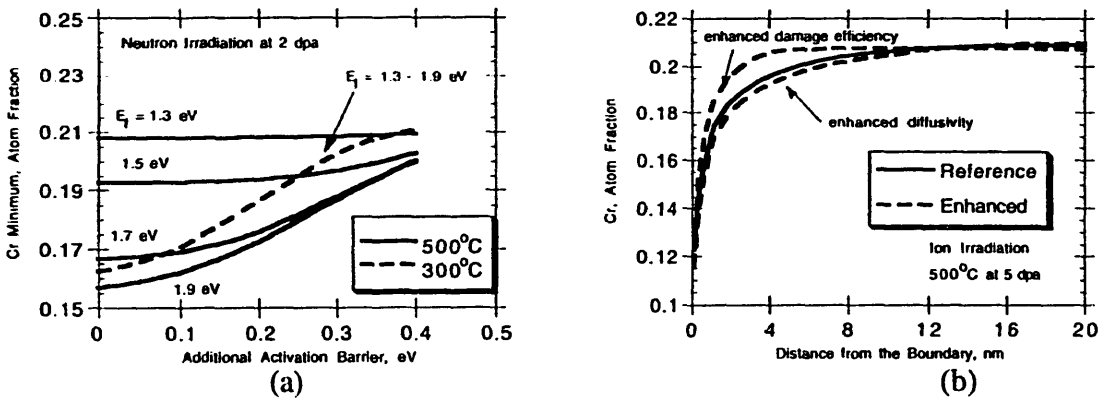

Figure 3. Effects of formation energy, E_f, for vacancies at grain boundaries and of the activation energy for jump of atoms and vacancies into a grain boundary at 300°C and at 500°C (a). Effect of an enhanced damage efficiency equal to 1.0 within 5 nm of the grain boundary and effect of an enhanced vacancy diffusivity in the near boundary region(b).

Near boundary regions may have defect characteristics different from far boundary regions because of local structure of grain boundaries and because of changing microchemistries within a few nms of the boundary. The damage efficiency may be enhanced near grain boundaries because the intracascade clustering and annihilation may be preempted by the close proximity of the grain boundary. A large increase (from 0.03 to 1.0) in the assumed local (5 nm) damage efficiency is seen in Figure 3b to be necessary to cause a significant influence on the predicted Cr depletion profile.

The effect of a ten-fold enhanced vacancy diffusion within 10 nm of the grain boundary is shown in Figure 3b. The principal effect is to reduce the local vacancy concentration which consequently induces a small depression in the Cr concentration near the boundary. A ten-fold increase in the near boundary diffusivity causes a slight reduction in the Cr minimum at the grain boundary and causes a slight increase in the width of the depletion profile.

MODEL COMPARISONS WITH MEASUREMENT

The predicted dose dependence of grain boundary Cr depletion for a damage efficiency of 0.03 is compared in Figure 4a with several FEG-STEM measurements (literature data compiled by Bruemmer et al. [8]) of grain boundary Cr depletion for boiling water reactor (BWR) irradiated austenitic stainless steels typical of 304SS. Predicted segregation trends are in accord with measured behavior, however, significant variability is observed in measured data. The dose dependence is dictated by the relaxation of the back diffusion kinetics, at first decreasing rapidly followed by a slow exponential approach to a steady-state composition. The wide variation in measured RIS is apparent in Figure 4a even for common alloy and irradiation type.

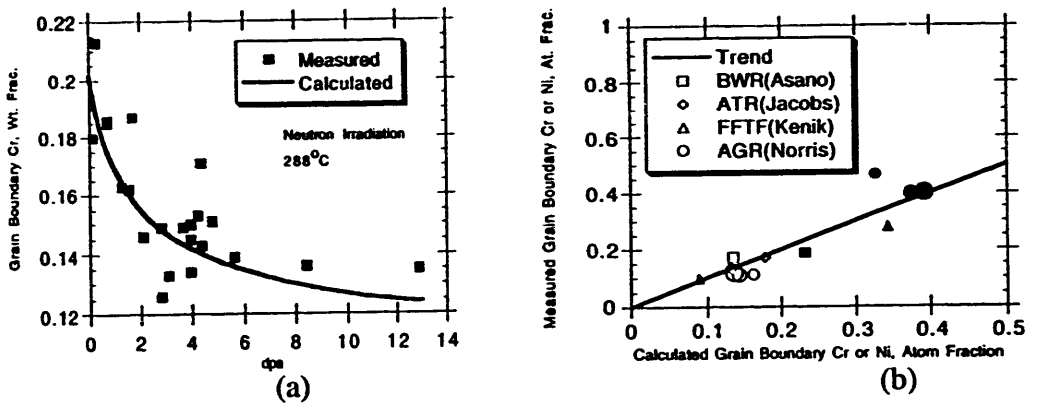

Figure 4. Comparison of calculated and measured grain boundary Cr concentration for BWR neutron irradiation at 288°C (a). Comparison of calculated and measured grain boundary compositions for the indicated irradiations (b). Open symbols represent Cr and closed symbols represent Ni. Larger symbols represent higher AGR temperatures shown in Table 1.

Table 1

Irradiation parameters and assumed bulk composition

Irradiation Type	Dose Rate dpa/s	Dose dpa	Temperature °C	Atom Fraction in Matrix Fe	Cr	Ni
BWR[9]	8×10^{-8}	8	288	0.690	0.205	0.105
ATR[10]	7×10^{-7}	4	288	0.695	0.230	0.075
FFTF[11]	5×10^{-7}	9	420	0.710	0.160	0.130
AGR[4]	1.2×10^{-8}	1	354	0.560	0.220	0.220
AGR[4]	2.5×10^{-8}	2	418	0.560	0.220	0.220
AGR[4]	3.2×10^{-8}	3	455	0.560	0.220	0.220
Ni++[5]	5×10^{-3}	5	500	0.706	0.207	0.087
Protons[12]	1.4×10^{-6}	1	400	0.706	0.207	0.087

In contrast to the 304SS alloys irradiated under similar conditions, RIS for a wide variety of austenitic alloys irradiated in a variety of reactors is shown in Figure 4b for a damage efficiency of 0.03. The measured Cr depletions and Ni enrichments are compared to predicted values for irradiations in the Advanced Gas-cooled Reactor (AGR) [4], a BWR [9], the Advanced Test Reactor (ATR) [10], and the Fast Flux Test Facility (FFTF) [11]. The assumed alloy composition and irradiation conditions are shown in Table 1. Three temperatures are shown for the AGR irradiation. The data qualitatively follow the trend line with scatter consistent with that observed in Figure 4a with the exception of the 354°C AGR irradiation. For constant neutron damage efficiency and material characteristic assumptions, the model provides a reasonable normalized interpretation of this diverse irradiation experience.

The effect of ion irradiation on RIS in model Fe-Cr-Ni alloys with additions of Si or P are shown in Figure 5. A damage efficiency of 0.03 was assumed for the Ni++ irradiation [5] and a damage efficiency of 0.2 was assumed for the proton irradiation [12]. For these assumptions, the model predictions underestimate the measured segregation for Ni++ irradiation and overestimate the measured segregation for proton irradiation.

DISCUSSION

Radiation-induced composition profiles at grain boundaries are controlled by both matrix characteristics and defect-boundary characteristics. Irradiation-induced atomic displacements in

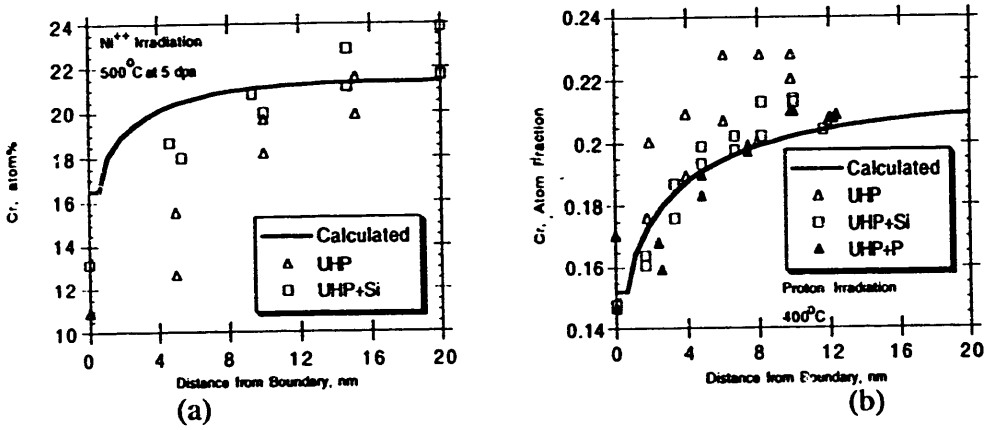

Figure 5. Calculated and measured Cr depletion at grain boundaries for Ni++ [5](a) and proton irradiation [12](b). The calculated boundary concentration is the FEG-STEM limit of resolution.

the matrix provide the potential for RIS but boundary characteristics can also have significant influences. The boundary influences are significant because back diffusion near the boundary strongly influences the composition profile. In the matrix far from the boundary, the defect concentrations are sufficiently high to promote effective back diffusion. The back (downhill) diffusion effectively counters the nonequilibrium (uphill) inverse-Kirkendall diffusion. Near the boundary, the vacancy concentration approaches values near zero and hence concentration gradients are kinetically stable. Boundary characteristics that influence the local vacancy concentration can strongly influence the local segregation profile.

Variations in observed segregation can arise from either defect interactions in the matrix or from defect interactions with grain boundaries. Assumptions of change in matrix characteristics result in similar changes in the RIS profile. Increasing the damage efficiency, increasing the vacancy mobility, and decreasing the matrix sink strength results in a deeper Cr depletion that extends over a larger distance from the boundary. For a given matrix potential for RIS, boundary characteristics can influence the local composition profiles. Boundary effects can strongly inhibit RIS, but can only weakly promote RIS.

Assumptions of vacancy interactions with grain boundaries result in large changes in the local concentration gradients. A lesser activation energy for formation of vacancies, and an additional activation energy for jump of vacancies into a boundary compared to in the matrix, both can result in significant elevation of the vacancy concentration which strongly promotes back diffusion. The back diffusion results in a lesser Cr concentration gradient and reduced RIS.

Boundary-defect interactions can be optimized by selecting damage rates and temperatures which maximize influences on near-boundary vacancy concentrations. Vacancy formation energy has greater influence for higher temperatures and lower damage rates. Conversely, the vacancy kinetic effect has greater influence for lower temperature and higher damage rates. Promoting faster vacancy diffusion, or increasing the damage efficiency, in the near-boundary region has only a minor influence of Cr concentration profiles. Vacancy gradients are steep near the boundary and, therefore, local production and annihilation of point defects do not strongly affect the local vacancy concentration.

Comparison of model predictions with neutron-induced RIS indicated that a damage efficiency of 0.03 was reasonable for a wide variety of neutron environments. An assumed proton irradiation damage efficiency of 0.2 (or less) was consistent with measured segregation data. Comparison of calculated and measured segregation induced by Ni++ ions indicated a damage efficiency greater than determined for neutron irradiation. An assumed damage efficiency of 0.03

for Ni^{++} irradiation underestimated the degree of Cr depletion, whereas an assumed damage efficiency of 0.2 for proton irradiation overestimated the degree of Cr depletion. The higher efficiency for proton irradiation compared to neutron irradiation was expected, but the apparent higher efficiency for Ni^{++} irradiation cannot be explained.

CONCLUSIONS

Defect-boundary interactions can play a critical role in radiation-induced grain boundary segregation. Although matrix characteristics control the potential for RIS, boundary characteristics can also influence segregation for nonequilibrium radiation effects. The cause for the boundary influence is that the concentration profiles that form near boundaries are steep and narrow because of restricted back diffusion within a few nanometers of the boundary. Vacancy processes such as thermal emission and activation for incorporation into a boundary were shown to cause significant reduction in the RIS behavior compared to perfect grain boundary sink assumptions.

ACKNOWLEDGMENTS

This research was support by the Materials Sciences Branch, Office of Basic Energy Sciences, U.S. Department of Energy, under Contract DE-AC06-76RLO 1830. Pacific Northwest Laboratory is operated for the DOE by Battelle Memorial Institute.

REFERENCES

1. Workshop on Solute Segregation and Phase Stability During Irradiation, edited by J. O. Stiegler, J. Nucl. Mater., **83** (1979).

2. R. A. Johnson and N. Q. Lam, Phys. Rev. B, vol **13**, no. 10, 4364 (1976).

3. A. D. Marwick, J. Phys. F, Metals Phys., **8**, 1849 (1978).

4. D. I. R. Norris, C. Baker and J. M. Titchmarsh, in Proceedings of Symposium on Radiation-Induced Sensitization of Stainless Steels, INIS-GB-90, ed. by D. I. R. Norris, Berkeley, Gloucestershire, GL13 9PB, Berkeley Nuclear Laboratories, 1981, p. 86.

5. E. P. Simonen and S. M. Bruemmer, in Corrosion '93 paper no. 615, National Association of Corrosion Engineers, Houston, TX., 1993.

6. J. M. Perks, A. D. Marwick and C. A. English, "A Computer Code to Calculate Radiation-Induced Segregation in Concentrated Ternary Alloys," AERE R 12121, Oxfordshire OX11 0RA, Harwell Laboratory, June 1986.

7. A. C. Hindmarsh, GEAR: Ordinary Differential Equation System Solver, Report UCID-30001, Rev. 3, Lawrence Livermore Laboratory, Livermore, CA, 1974.

8. S. M. Bruemmer and E. P. Simonen, ibid 5, paper no. 616.

9. K. Asano, K. Fukuya, K. Nakata and M. Kodama, in 5th International Symposium on Environmental Degradation of Materials in Nuclear Power Systems - Water Reactors, Monterey, CA, ANS, La Grange Park, IL, 1992, p. 838.

10. A. J. Jacobs, C. M. Shepard, G. E. C. Bell, and G. P. Wozadlo, ibid 9, p. 917.

11. E. A. Kenik, T. Inazumi and G. E. C. Bell, J. Nucl. Mater., **183**, 145 (1991).

12. R. D. Carter, D. L. Damcott, M. Atzmon, G. S. Was and E. A. Kenik, J. Nucl. Mater., **205**, 361 (1993).

DATE
FILMED
3/11/94
END